Supporting Material

Secondary structure propensities in peptide folding simulations: A systematic comparison of molecular mechanics interaction schemes

Dirk Matthes and Bert L. de Groot

Supporting Material

1 Methods

Model Peptides

Five, small peptides where chosen for the comparison study, which adopt prototypic secondary structure elements in solution and are well characterized, both experimentally and with MD simulations.

Chignolin

The 10 residue β-hairpin peptide Chignolin was designed by statistical considerations (1) and characterized by nuclear magnetic resonance (NMR) and circular dichroism (CD) experiments in solution. The molar fraction of folded peptide at 300 K was determined to approximately 60 %. Chignolin was also subject of numerous computational studies and the NMR-structure was reproduced by MD from the extended state (2–7).

Mbh12

The sequence for the Mbh12 peptide stems from a combinatorial approach to de novo design a stable β-hairpin fold in a linear peptide (8). CD and NMR experiments identified a percentage of β-hairpin structure higher than 66% at 278 K.

Trp-cage (Tc5b)

The Trp-cage is a 20 residue peptide designed and first characterized by Neidigh et al. (9). The sequence was optimized by mutation and folds into a compact structure consisting of a N-terminal α-helix, a 3_{10}-helix and a hydrophobic core formed by Trp, Tyr and Pro residues. The Tc5b mutant used in this study was found to be folded to > 95 % in aqueous solution and melts at 315 K as determined by CD and NMR (9). The Trp-cage is considered a model system for folding simulations, displaying two-state folding properties and a folding time in the microsecond regime (10). Tc5b has been thoroughly studied by molecular dynamics and numerous reports of folding simulations since then have contributed to the understanding of structural features, which govern fold stabilization and facilitation of the fast folding (11–15).

Fs$_{21}$

Originally designed by Lockhart et al. to asses electrostatic interactions in α-helices, the 21 residue polyalanine peptide Fs-NH$_2$ became a popular model system for helix-coil transition and is well studied, both experimentally (16–21) and by MD simulations (22–29). Based on CD spectra signatures the peptide was reported to be > 90 % helical in aqueous solution at 273 K (16). Controversial data is available concerning the melting temperature. The melting point was reported at 308 K (16) and 303 K (19) in studies using CD, while infrared spectroscopy experiments observed a larger melting temperature of 334 K, but cannot distinguish between α- and 3_{10}-helix (18). Note that depending on the experimental setup different N-terminal capping groups were used.

Agd1 (de novo)

We decided to include another helical peptide and constructed a short peptide sequence with a high helical propensity using the AGADIR prediction algorithm (30), which is based on the empirical analysis of experimental data. We derived a 13 amino acids long peptide sequence (here termed Agd1), whose predicted helical content with protected N- and C-termini under conditions of pH 7 and 300 K is calculated to be 50 %.

Force Field Settings

For the comparsion of force fields, we focused on variants as implemented in the GROMACS simulation software suite:

The AMBER99SB force field (ff99SB) (31) is based on the AMBER99 force field (32), with new parameters for backbone dihedrals to achieve a better balance of secondary structure elements. The AMBER03 force field (ff03) (33) is also a variant of the AMBER99 potential with rederived charges and main-chain torsion potentials, introducing unique main-chain charges for each amino acid. The OPLS-AA/L force

field (OPLS) (34) was parameterized for liquid state thermodynamics and later improved by refitting the torsion/backbone parameters from quantum chemical calculations (35). The GROMOS96 (G96) united atom force field is continuously improved and refined. Popular examples are the G96 43A1 (36, 37) and the G96 53A6 force field (38, 39), with the latter being the newest parameter set with adjusted partial charges to better reproduce hydration free enthalpies in water.

All simulations were carried out using electrostatic schemes as originally used for development and in addition, the Particle Mesh Ewald (PME) (40, 41) method for comparison.

The long-range and slowly decaying coulomb potential still poses the most challenging problem to solve in MD simulations, both in terms of accuracy and computational effort. Several methods have been introduced to make the calculation of the non-bonded interactions in biomolecular systems feasible. Cutoff methods simply neglect the contributions from the electrostatic interactions beyond a certain cutoff distance. Satisfactory accuracy without making severe errors is not expected, even for large cutoff distances. With the continuum based reaction-field (RF) (42) approach, charge-charge interactions are calculated explicitly within a sphere of a given radius and beyond by assuming a homogeneous medium with a certain dielectric constant. The PME method derives the electrostatic forces in a periodic system by splitting the potential into two separate summation terms. These terms describe the short-range (direct space)and long-range (reciprocal space) part of the coulomb potential. Both rapidly converge and therefore can be truncated at a cutoff without losing much accuracy. For an efficient calculation of the long-range part, the continuous charge positions are substituted by a mesh-based charge density that a fast fourier transformation can be used to perform the necessary transformation to reciprocal space.

The MD simulations for each peptide system were performed using eight combinations of force fields, water models and methods for treating the long-range electrostatic interactions. The cutoff distances for the non-bonded interactions which were used with the different force fields are summarized in Table S1.

System	Force field	Electrostatic scheme	VdW scheme	Water model
ff03-PME	AMBER03 (33)	PME (1.0 nm)	Cutoff (0.8 nm)	TIP3P
ff99SB-PME	AMBER99SB (31)	PME (1.0 nm)	Cutoff (0.8 nm)	TIP3P
43A1-RF	GROMOS96 43A1 (36, 37)	Reaction-Field (1.4 nm)	Cutoff (1.4 nm)	SPC
43A1-PME	GROMOS96 43A1	PME (0.9 nm)	Cutoff (1.4 nm)	SPC
53A6-RF	GROMOS96 53A6 (38, 39)	Reaction-Field (1.4 nm)	Cutoff (1.4 nm)	SPC
53A6-PME	GROMOS96 53A6	PME (0.9 nm)	Cutoff (1.4 nm)	SPC
OPLS-Cutoff	OPLS-AA/L (34, 35)	Cutoff (1.4 nm)	Cutoff (1.4 nm)	TIP4P
OPLS-PME	OPLS-AA/L	PME (0.9 nm)	Cutoff (1.4 nm)	TIP4P

Table 1: Force field setting and treatment of non-bonded interactions

2   Averaged Root Mean-Square Deviation (RMSD)

We performed an analysis of the root mean-square deviations (RMSD) for the peptides with experimentally determined native state (Chignolin, Mbh12 and Tc5b). Averaged RMSDs for the main chain and C_β atom coordinates of these three peptides to the respective NMR reference structure as function of simulation time are summarized in Table S2. An average RMSD for each of the trajectories was calculated over the last 225 ns. The RMSD values of the additional, three shorter Tc5b simulations were averaged over the last 15 ns. To better indicate the trend of the performed simulations, we also list the averaged RMSDs of the final 5 ns of each trajectory in parentheses, respectively.

The corresponding average RMSDs range from 0.15 to 0.3 nm (see Table S2).Particularly low deviations from the reference structure are found with ff99SB (0.13 nm), OPLS-PME and ff03 (0.14 nm) for the CHI.REF simulations. Results obtained for the simulations started from an extended peptide chain (CHI) are not only dependent on the structural similarity of the folded state to the reference, but additionally on how fast and efficient the conformational space was sampled towards the reference conformation. The Chignolin peptide is folded to a structure very close to the experimentally determined one, for example with the ff99SB (0.13 nm) and ff03 (0.22 nm), respectively. A high structural stability from the prefolded state and fast sampling towards the reference therefore led to the overall smallest average RMSDs in both AMBER force fields, irrespective of the initial configuration.

A different scenario arises from the simulations starting from the extended chain of the Mbh12 peptide (MBH). Hairpin formation took place rather fast in all studied G96 and OPLS force field variants. The peptide conformations were also stable from the reference structure for this group of force fields over the simulated 250 ns (Table S2).

The Tc5b simulations were only started from the reference NMR structure. In addition to one simulation of 250 ns, three independent runs of 30 ns were conducted in order to check for statistical significance of our results. All four simulations approached similar averaged RMSDs in the different force fields, respectively (Table S2).

System	average main-chain and C_β RMSD [nm]							
	CHI	CHI.REF	MBH	MBH.REF	TC5B.REF	TC5B.REF.A	TC5B.REF.B	TC5B.REF.C
ff03-PME	0.22 (0.22)	0.13 (0.32)	0.58 (0.53)	0.53 (0.46)	0.21 (0.22)	0.15 (0.18)	0.13 (0.17)	0.30 (0.35)
ff99SB-PME	0.15 (0.16)	0.13 (0.14)	0.53 (0.45)	0.38 (0.44)	0.12 (0.10)	0.10 (0.10)	0.12 (0.13)	0.13 (0.12)
43A1-RF	0.30 (0.20)	0.26 (0.20)	0.34 (0.37)	0.32 (0.35)	0.35 (0.45)	0.39 (0.42)	0.41 (0.39)	0.30 (0.38)
43A1-PME	0.30 (0.23)	0.27 (0.33)	0.42 (0.38)	0.31 (0.26)	0.40 (0.46)	0.24 (0.24)	0.42 (0.42)	0.30 (0.24)
53A6-RF	0.30 (0.15)	0.23 (0.29)	0.44 (0.52)	0.25 (0.29)	0.48 (0.52)	0.29 (0.28)	0.38 (0.38)	0.40 (0.40)
53A6-PME	0.44 (0.23)	0.21 (0.28)	0.33 (0.27)	0.25 (0.21)	0.57 (0.52)	0.42 (0.48)	0.45 (0.44)	0.38 (0.34)
OPLS-Cutoff	0.52 (0.62)	0.33 (0.34)	0.50 (0.50)	0.22 (0.17)	0.22 (0.22)	0.25 (0.38)	0.24 (0.29)	0.25 (0.29)
OPLS-PME	0.56 (0.61)	0.14 (0.13)	0.33 (0.31)	0.22 (0.24)	0.20 (0.25)	0.19 (0.20)	0.17 (0.20)	0.20 (0.22)

Table 2: Root Mean-Square Deviations from NMR reference structures as an average for each trajectory (average RMSDs over the final 5 ns of each simulation are given in parentheses)

3 Nuclear Overhauser Enhancement (NOE)

For the studied peptides the following number of NOE restraints were available from NMR, listed according to the above explained distance measure. These include short-range restraints between atoms on neighboring residues and intra-residual atoms. Medium- and long-range restraints are defined when the atom pairs are separated by two to four, and five or more residues in the sequence, respectively. Chignolin (172) - 110 short, 24 medium, 38 long (1, 2); Mbh12 (60) - 18 short, 6 medium, 36 long (8); Tc5b (159) - 105 short, 36 medium, 28 long (9). For Chignolin and Tc5b the minority of the NOEs reports on the global, long-range structure, whereas for Mbh12 mainly long-range distance restraints were assigned. For polypeptide conformations that transcend these long distance restraints and therefore violate the overall, secondary or tertiary fold, one expects the largest NOE violations.

4 DSSP Analysis

The secondary structure element is color coded according to the figure legend and is plotted against the simulation time. Vertical coordinate represents the residue number of the respective peptide. The caption denotes the starting structure of the model peptide and the employed force field variant, respectively (see methods). For each simulation representative structures are shown, extracted at 0 ns, 50 ns, 150 ns and 250 ns.

Chignolin

(a) CHI - ff03-PME

(b) CHI - ff99SB-PME

(c) CHI - 43A1-RF

(d) CHI - 43A1-PME

(e) CHI - 53A6-RF

(f) CHI - 53A6-PME

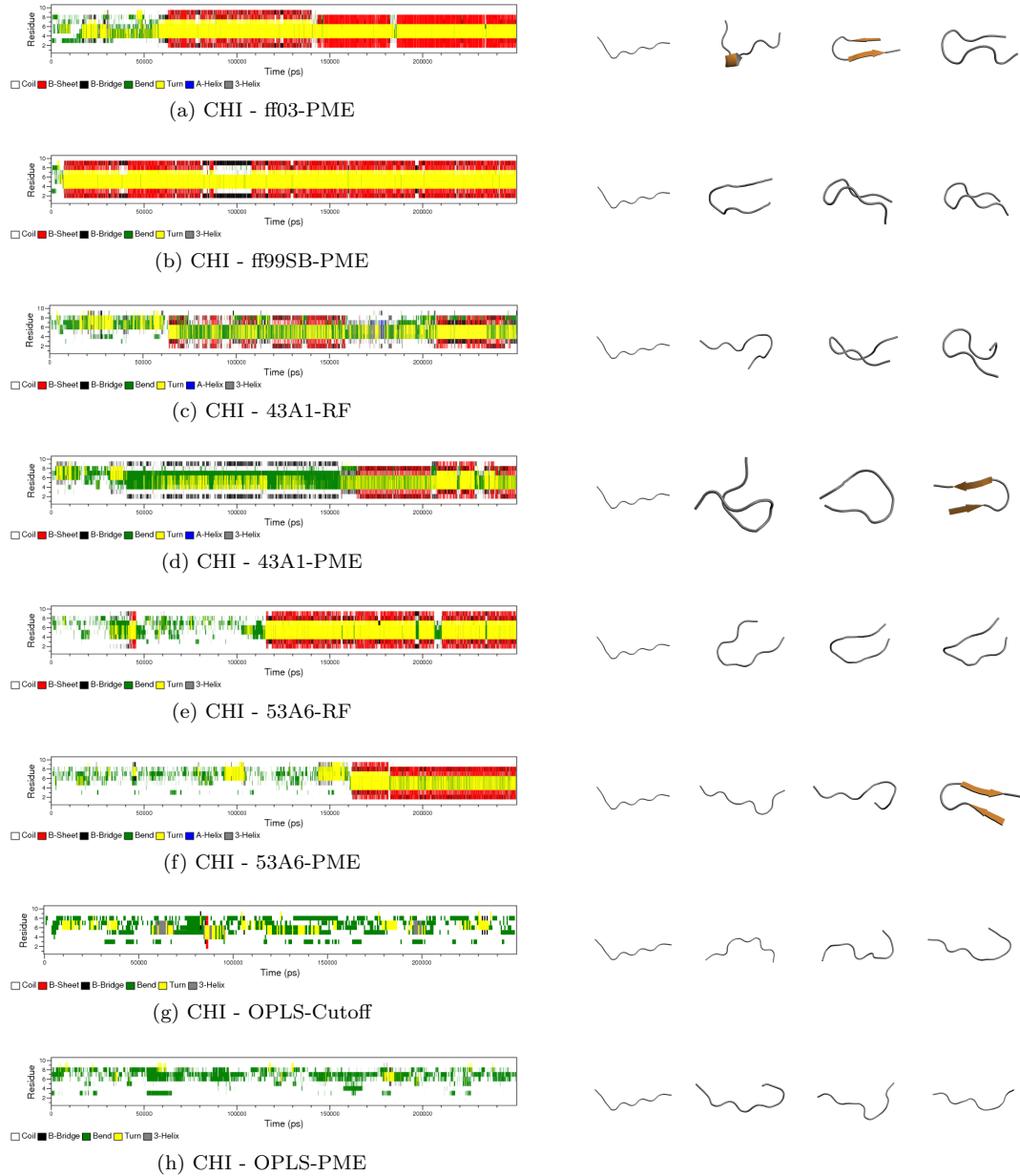(g) CHI - OPLS-Cutoff

(h) CHI - OPLS-PME

Figure 1: Evolution of the secondary structure elements with simulation time in the various force fields for the CHI trajectories. Representative structures shown at 0 ns, 50 ns, 150 ns and 250 ns.
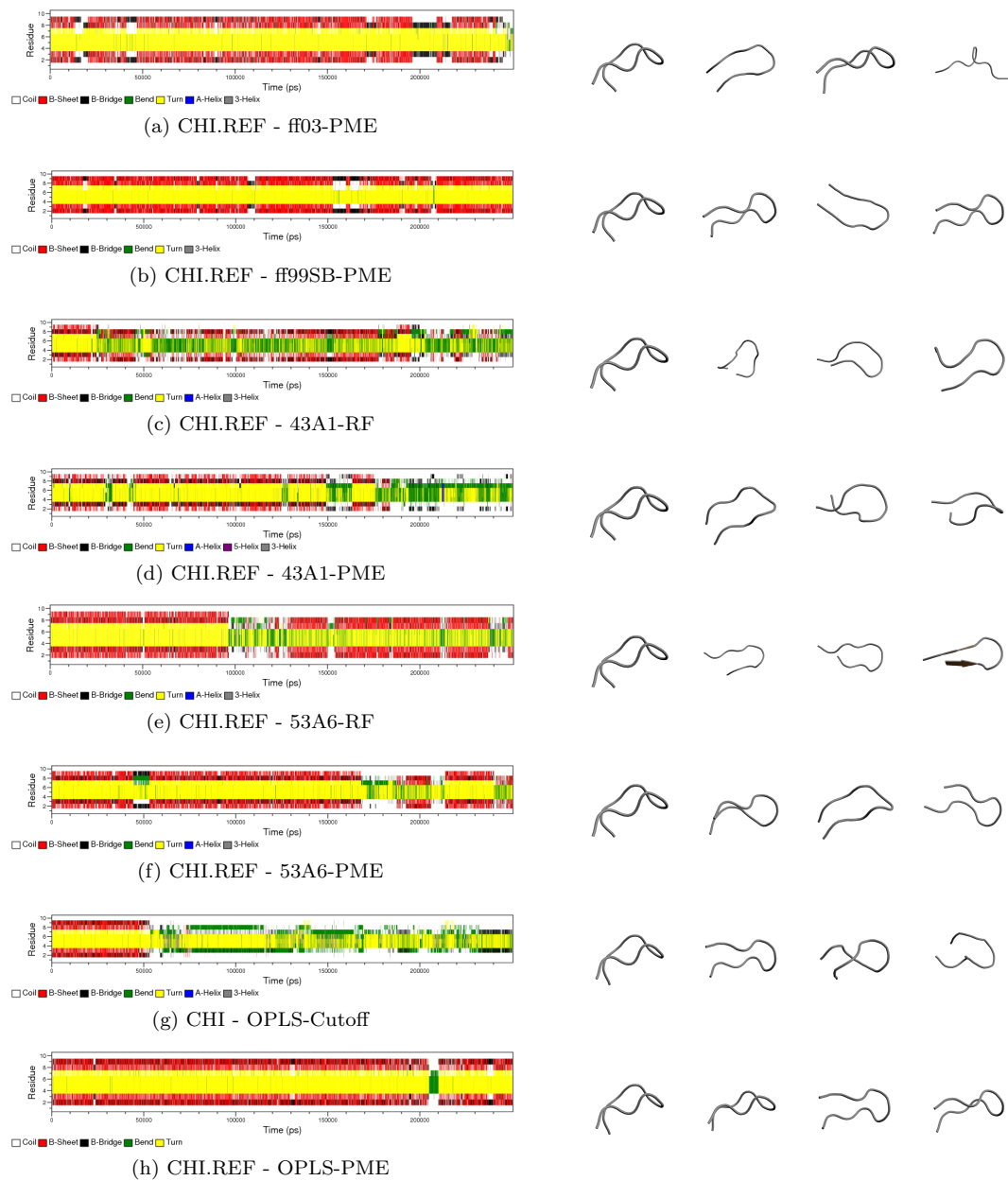
Figure 2: Evolution of the secondary structure elements with simulation time in the various force fields for the CHI.REF trajectories. Representative structures shown at 0 ns, 50 ns, 150 ns and 250 ns.
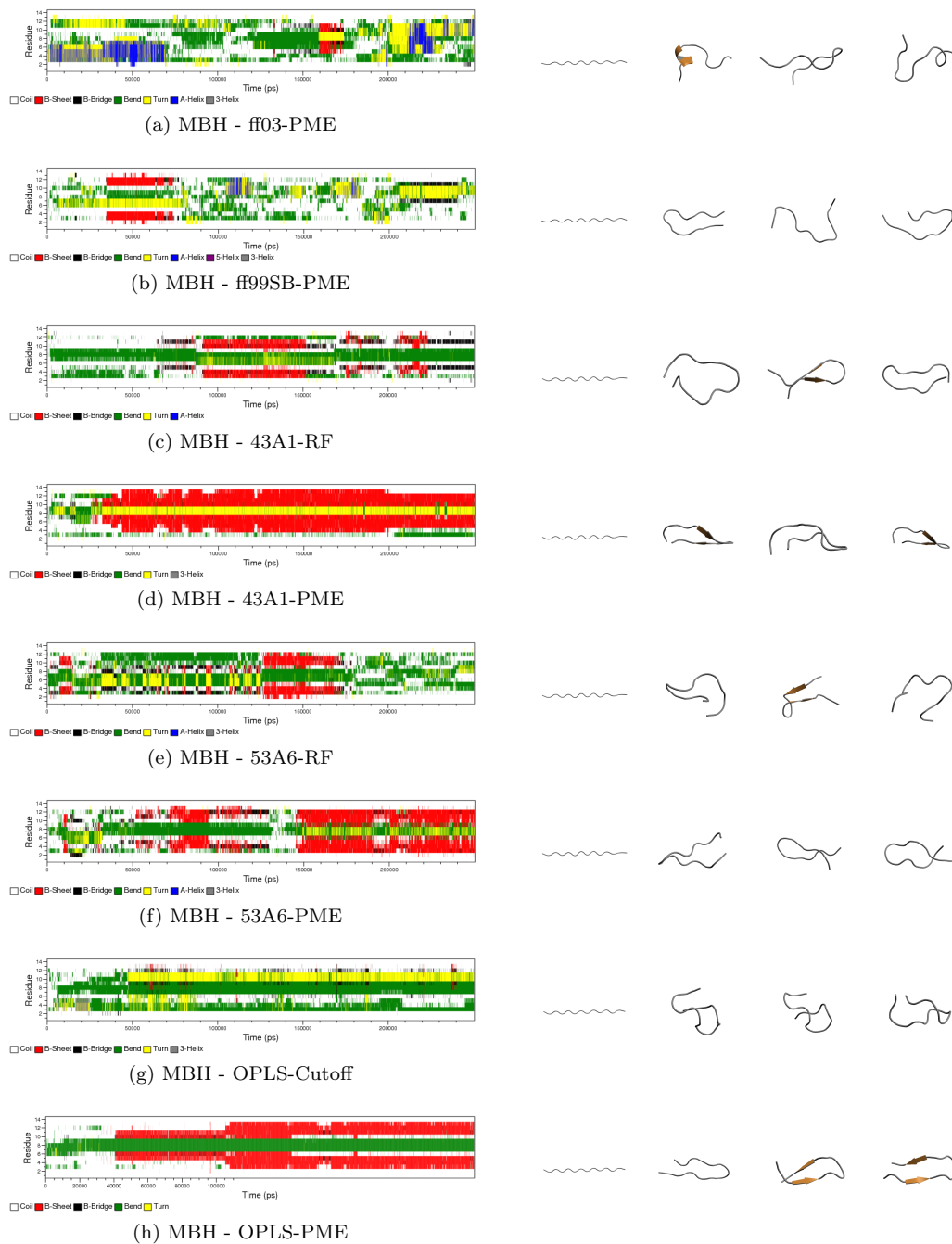
Mbh12

(a) MBH - ff03-PME

(b) MBH - ff99SB-PME

(c) MBH - 43A1-RF

(d) MBH - 43A1-PME

(e) MBH - 53A6-RF

(f) MBH - 53A6-PME

(g) MBH - OPLS-Cutoff

(h) MBH - OPLS-PME

Figure 3: Evolution of the secondary structure elements with simulation time in the various force fields for the MBH trajectories. Representative structures shown at 0 ns, 50 ns, 150 ns and 250 ns.
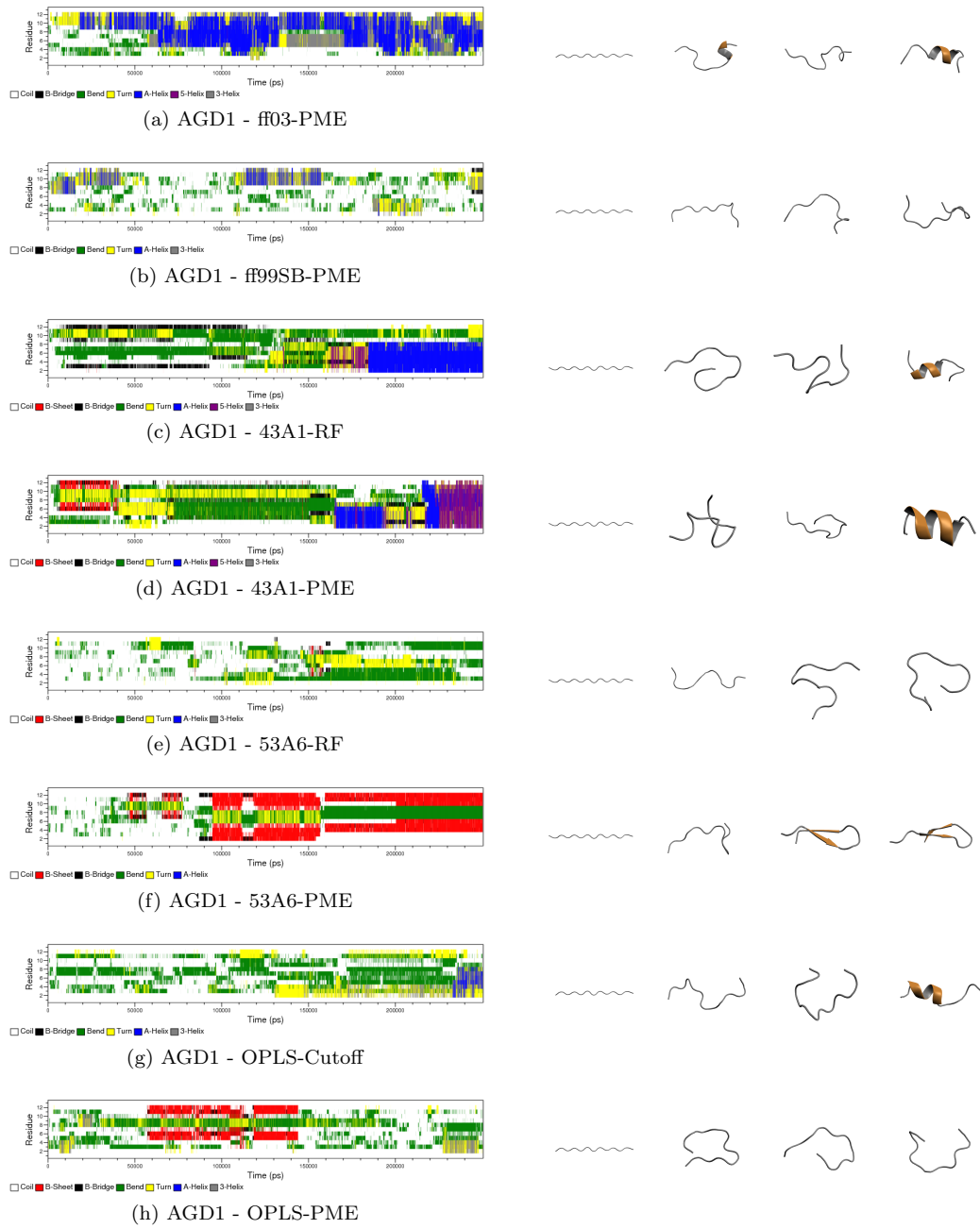
(a) MBH.REF - ff03-PME

(b) MBH.REF - ff99SB-PME

(c) MBH.REF - 43A1-RF

(d) MBH.REF - 43A1-PME

(e) MBH.REF - 53A6-RF

(f) MBH.REF - 53A6-PME

(g) MBH.REF - OPLS-Cutoff

(h) MBH.REF - OPLS-PME

Figure 4: Evolution of the secondary structure elements with simulation time in the various force fields for the MBH.REF trajectories. Representative structures shown at 0 ns, 50 ns, 150 ns and 250 ns.

Agd1

(a) AGD1 - ff03-PME

(b) AGD1 - ff99SB-PME

(c) AGD1 - 43A1-RF

(d) AGD1 - 43A1-PME

(e) AGD1 - 53A6-RF

(f) AGD1 - 53A6-PME

(g) AGD1 - OPLS-Cutoff

(h) AGD1 - OPLS-PME

Figure 5: Evolution of the secondary structure elements with simulation time in the various force fields for the AGA trajectories. Representative structures shown at 0 ns, 50 ns, 150 ns and 250 ns.
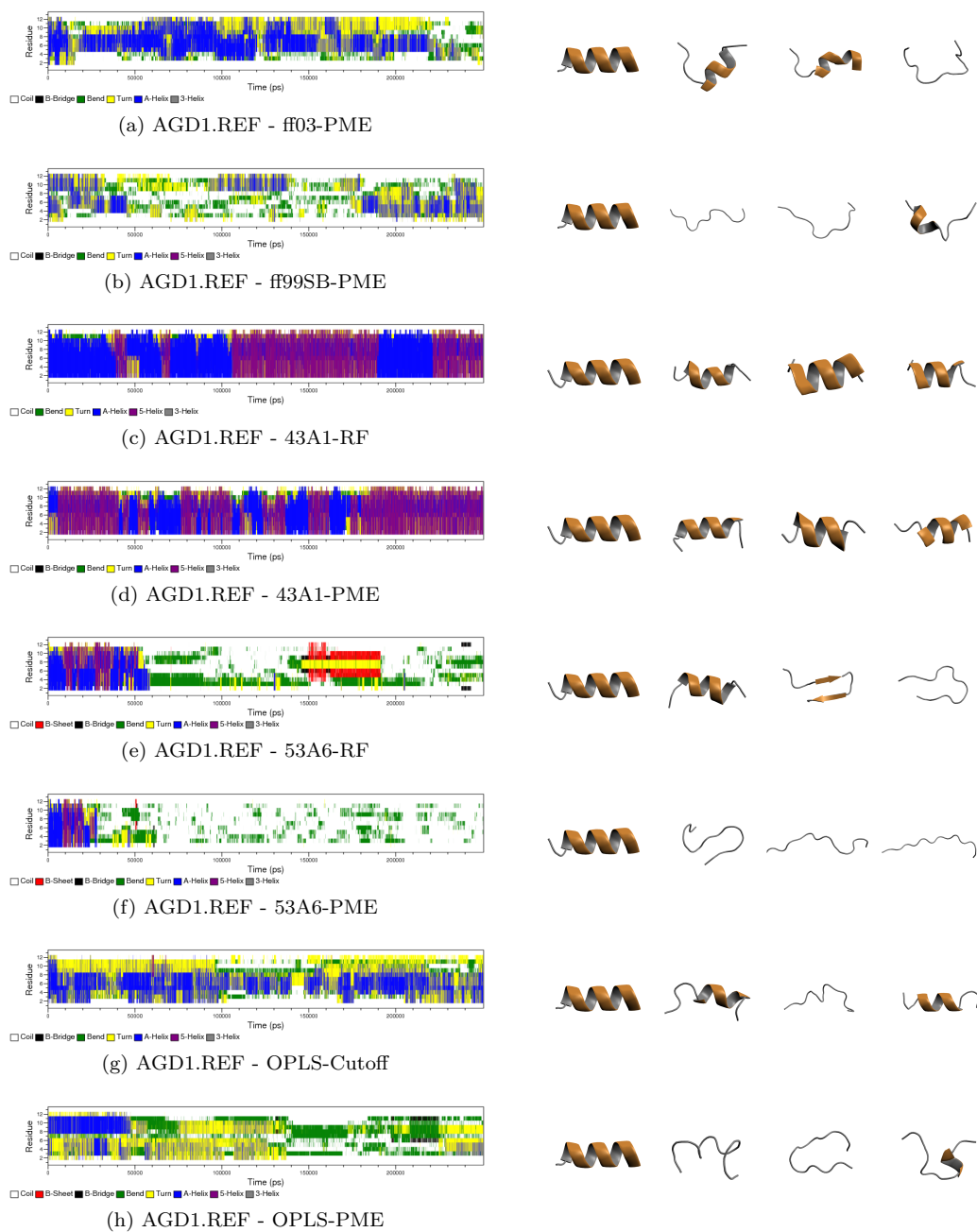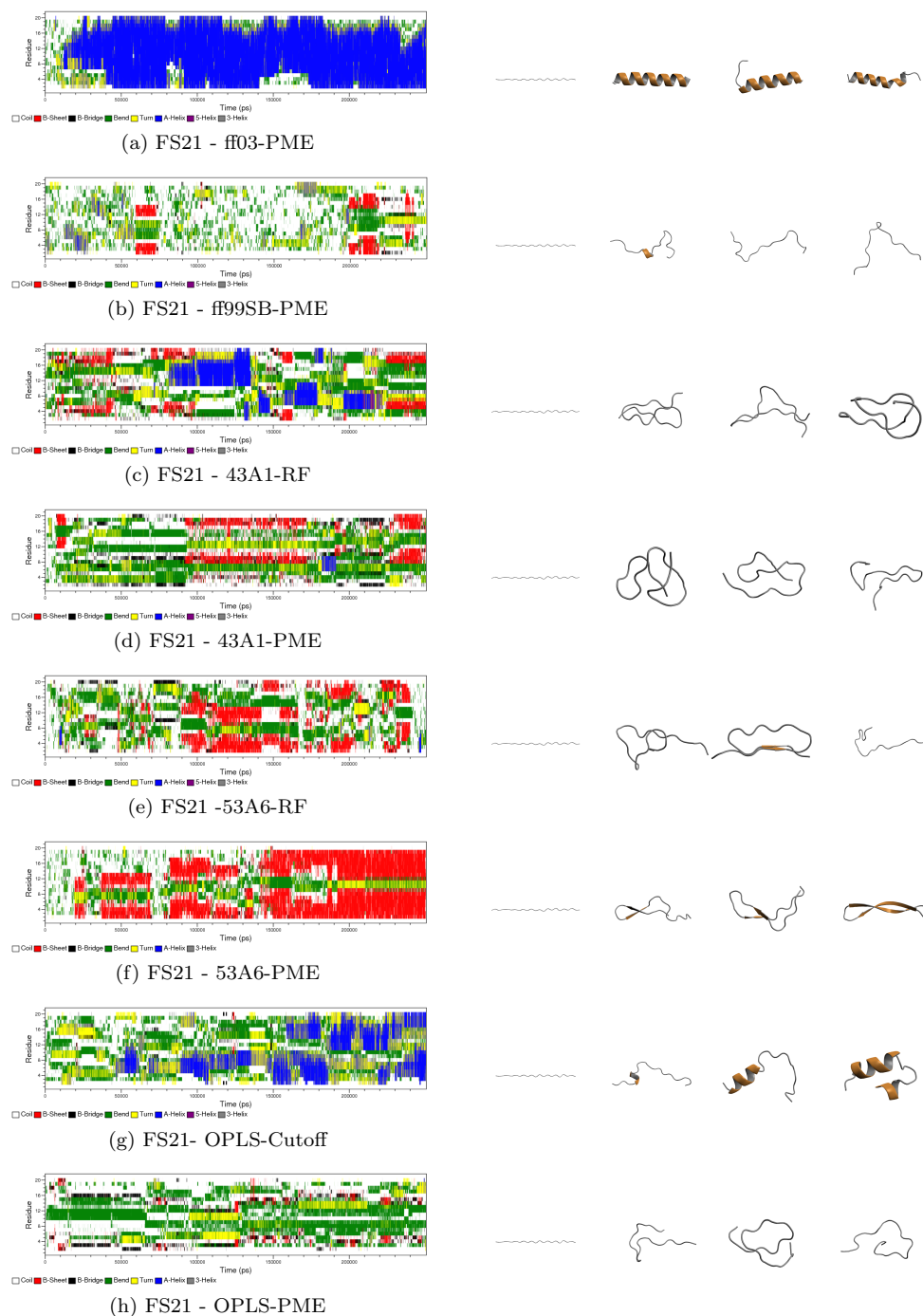
(a) AGD1.REF - ff03-PME

(b) AGD1.REF - ff99SB-PME

(c) AGD1.REF - 43A1-RF

(d) AGD1.REF - 43A1-PME

(e) AGD1.REF - 53A6-RF

(f) AGD1.REF - 53A6-PME

(g) AGD1.REF - OPLS-Cutoff

(h) AGD1.REF - OPLS-PME

Figure 6: Evolution of the secondary structure elements with simulation time in the various force fields for the AGA.REF trajectories. Representative structures shown at 0 ns, 50 ns, 150 ns and 250 ns.

Fs$_{21}$

(a) FS21 - ff03-PME

(b) FS21 - ff99SB-PME

(c) FS21 - 43A1-RF

(d) FS21 - 43A1-PME

(e) FS21 -53A6-RF

(f) FS21 - 53A6-PME

(g) FS21- OPLS-Cutoff

(h) FS21 - OPLS-PME

Figure 7: Evolution of the secondary structure elements with simulation time in the various force fields for the FS trajectories. Representative structures shown at 0 ns, 50 ns, 150 ns and 250 ns.
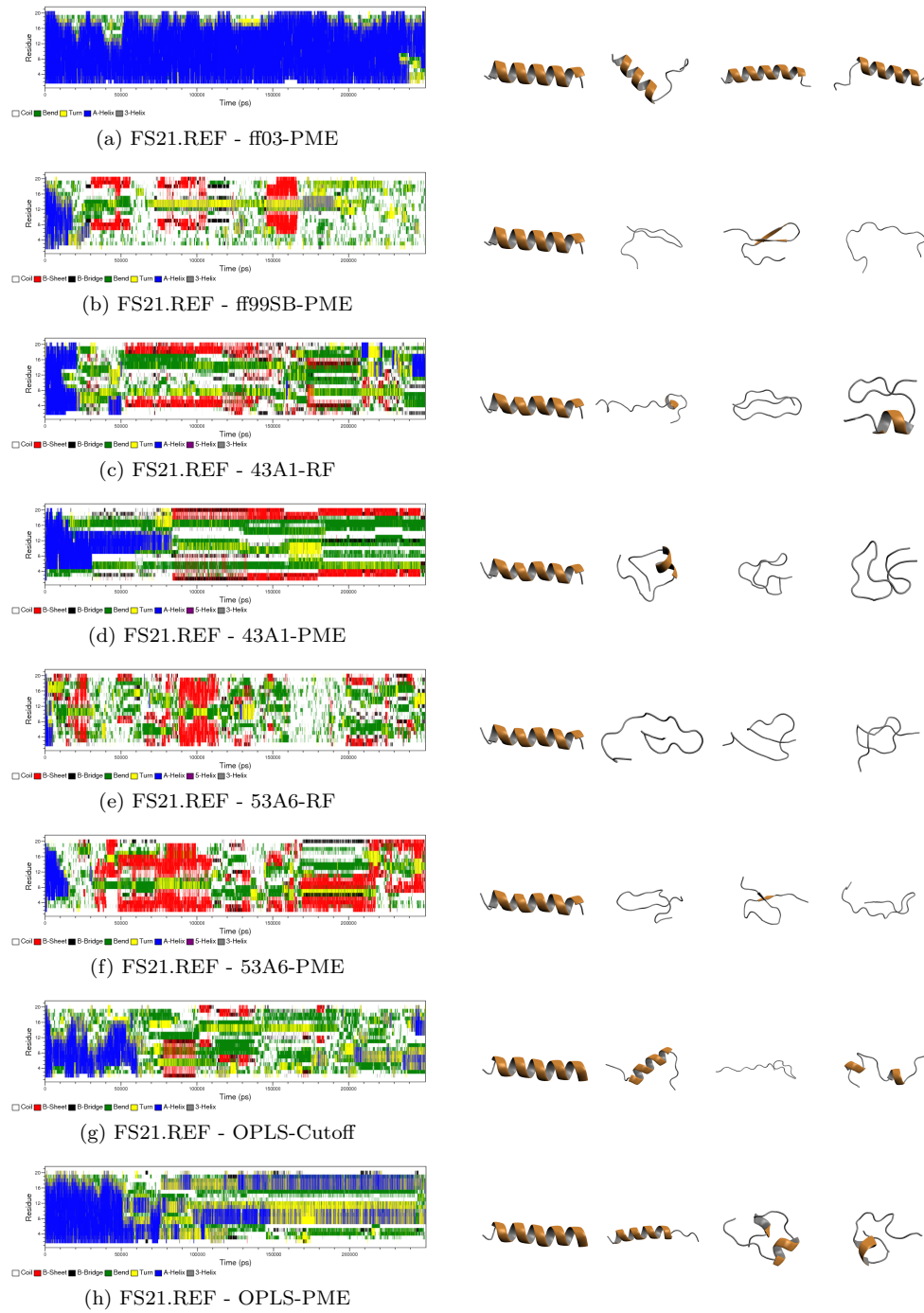
(a) FS21.REF - ff03-PME

(b) FS21.REF - ff99SB-PME

(c) FS21.REF - 43A1-RF

(d) FS21.REF - 43A1-PME

(e) FS21.REF - 53A6-RF

(f) FS21.REF - 53A6-PME

(g) FS21.REF - OPLS-Cutoff

(h) FS21.REF - OPLS-PME

Figure 8: Evolution of the secondary structure elements with simulation time in the various force fields for the FS.REF trajectories. Representative structures shown at 0 ns, 50 ns, 150 ns and 250 ns.
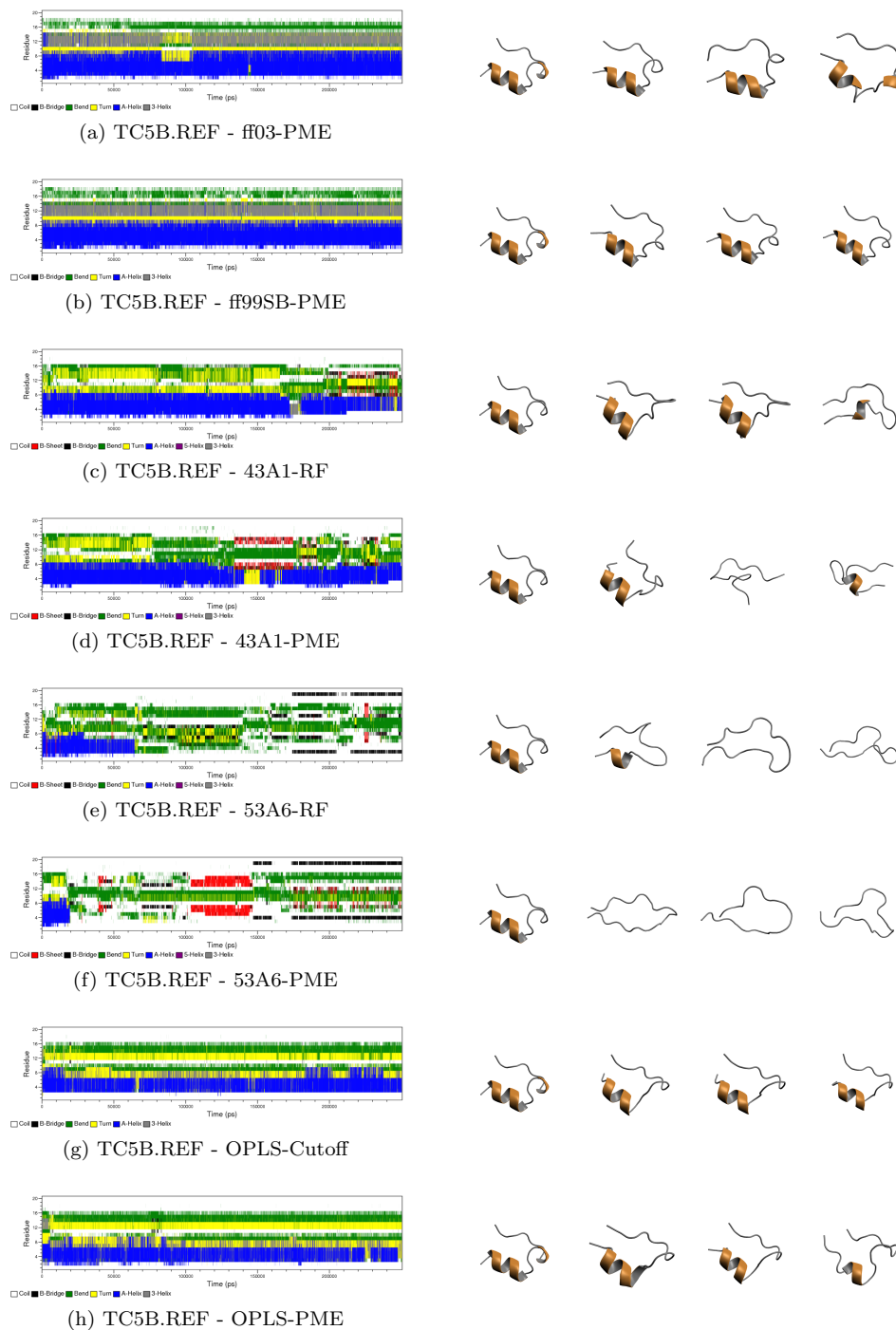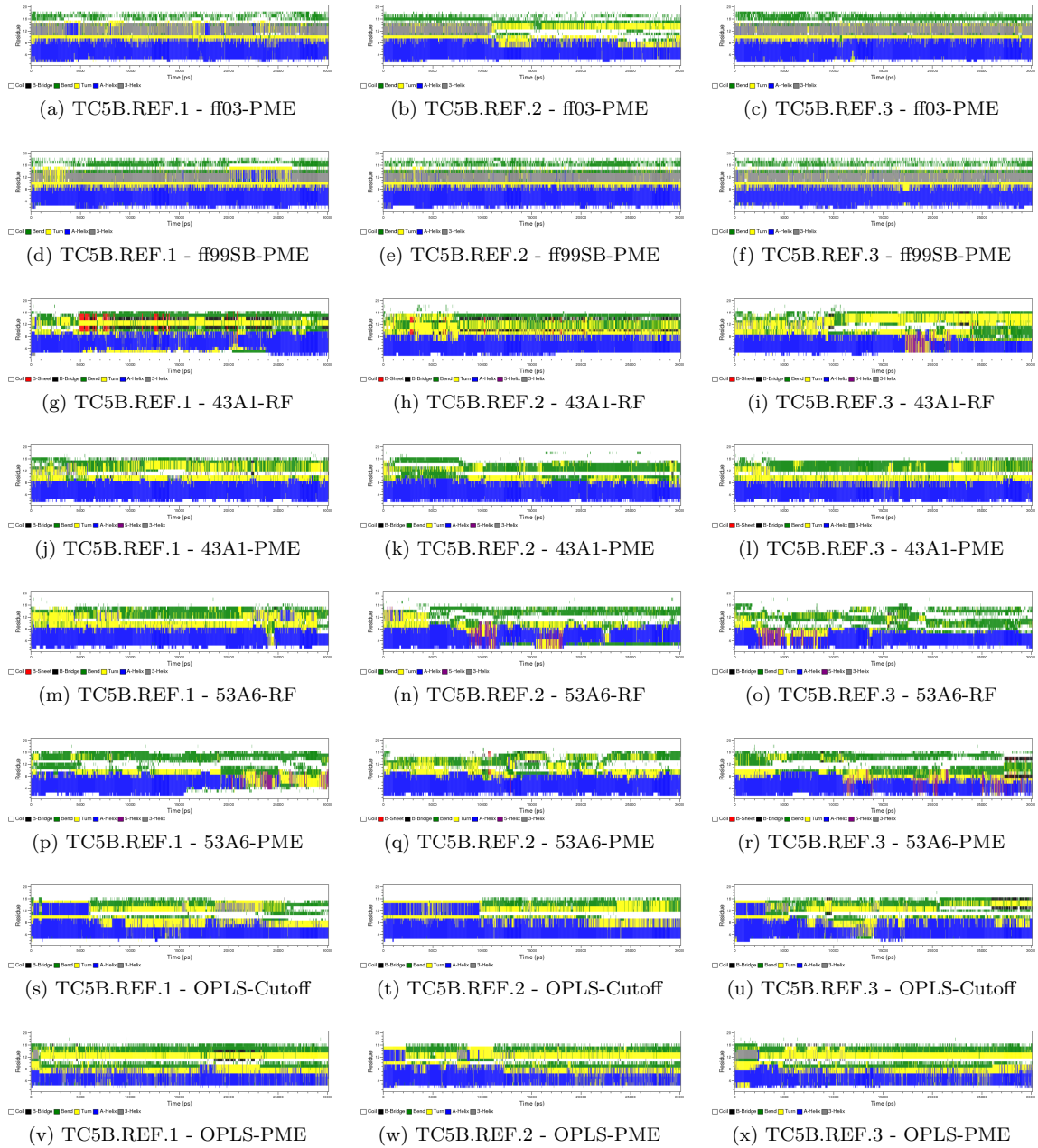
Trp-cage - TC5B.REF (250 ns)

(a) TC5B.REF - ff03-PME

(b) TC5B.REF - ff99SB-PME

(c) TC5B.REF - 43A1-RF

(d) TC5B.REF - 43A1-PME

(e) TC5B.REF - 53A6-RF

(f) TC5B.REF - 53A6-PME

(g) TC5B.REF - OPLS-Cutoff

(h) TC5B.REF - OPLS-PME

Figure 9: Evolution of the secondary structure elements with simulation time in the various force fields for the TC5B.REF (250 ns) trajectories. Representative structures shown at 0 ns, 50 ns, 150 ns and 250 ns.

Trp-cage - TC5B.REF (30 ns)

(a) TC5B.REF.1 - ff03-PME

(b) TC5B.REF.2 - ff03-PME

(c) TC5B.REF.3 - ff03-PME

(d) TC5B.REF.1 - ff99SB-PME

(e) TC5B.REF.2 - ff99SB-PME

(f) TC5B.REF.3 - ff99SB-PME

(g) TC5B.REF.1 - 43A1-RF

(h) TC5B.REF.2 - 43A1-RF

(i) TC5B.REF.3 - 43A1-RF

(j) TC5B.REF.1 - 43A1-PME

(k) TC5B.REF.2 - 43A1-PME

(l) TC5B.REF.3 - 43A1-PME

(m) TC5B.REF.1 - 53A6-RF

(n) TC5B.REF.2 - 53A6-RF

(o) TC5B.REF.3 - 53A6-RF

(p) TC5B.REF.1 - 53A6-PME

(q) TC5B.REF.2 - 53A6-PME

(r) TC5B.REF.3 - 53A6-PME

(s) TC5B.REF.1 - OPLS-Cutoff

(t) TC5B.REF.2 - OPLS-Cutoff

(u) TC5B.REF.3 - OPLS-Cutoff

(v) TC5B.REF.1 - OPLS-PME

(w) TC5B.REF.2 - OPLS-PME

(x) TC5B.REF.3 - OPLS-PME

Figure 10: Evolution of the secondary structure elements with simulation time in the various force fields for the TC5B.REF (30 ns) trajectories.

5 Backbone Dihedral Analysis

The apparent differences in structural representation of the polyalanine peptide Fs_{21} indicated that it might prove insightful to examine the backbone conformations in terms of sampled distributions of torsion angles ϕ (C-N-C_α-C) and ψ (N-C_α-C-N).

We chose to evaluate the torsional sampling of alanine residues, which are only present in Fs_{21} among the tested model peptides, and glycine and proline, as these are the most abundant in the simulated model peptide sequences.

Histogram analysis was used to calculate normalized density plots of dihedral pairs (ϕ/ψ) over all trajectories produced by each force field, respectively. We then qualitatively compared occupancy and relative sampling of ϕ/ψ dihedral pairs. The major low-energy regions in the Ramachandran plot, which are characteristic for prominent secondary structure elements are are shown in Fig. S11: right-handed α-helix (α_R: -70° ± 30°, -50° ± 30°), left-handed α-helix (α_L: +50 ± 30°, +50° ± 30°), polyproline II (PP_{II}: -70° ± 30°, +150° ± 30°) and extended β basin (β: -150° ± 30°, +150° ± 30°) (43–45).
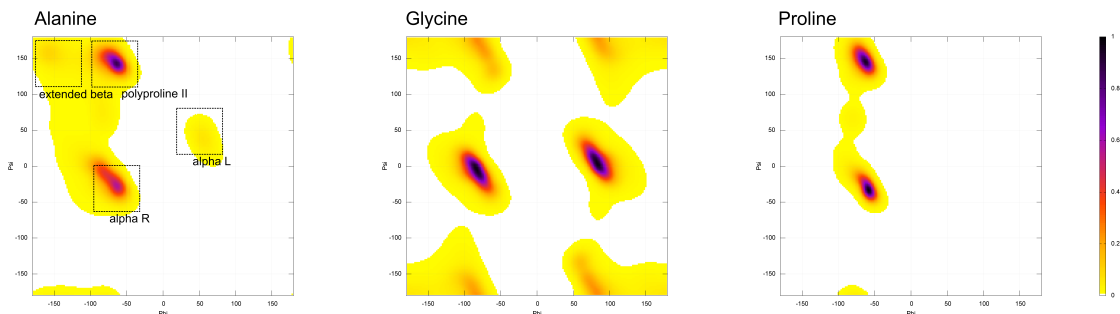

Figure 11: Normalized ϕ/ψ histogram plot for alanine, glycine and proline residues obtained from dihedral analysis of 500 high-resolution protein structures (45).

For the alanine aminoacids of the Fs_{21} peptide all force fields sampled the principal regions, except for ff03, where the α_L basin is not visited and the β region only to very small extent (Fig. S12). The α_L basin is visited most with the ff99SB force field and the relative ϕ/ψ distributions are comparable to the Ramachandran map obtained from statistical analysis of alanine backbone conformations in 500 high-resolution protein structures (Fig. S11) (45). In the OPLS trajectories similar favorable regions were sampled, except for the dihedral pairs in the range of -125° ± 30°, +75° ± 30°, which are not present in the ff99SB data. In all simulations carried out with the GROMOS96 force fields, the α_L is visible as a broad feature over a large ψ range. The β and PP_{II} regions appear as four dense states, which are particularly high populated in 53A6 and deviate from the empirical dihedral distribution from protein structure validation (45).

The histogram plots for the achiral glycine residues are asymmetric because of the influence of chiral centers in neighboring residues, and left-handed helix regions are therefore more densely populated. Moreover, a large number of dihedral pairs is allowed without the steric hindrance of a C_β, compared to all other amino acids.

Markedly, the extended β- and α_L-regions are strongly sampled in the OPLS simulations, but within a very narrow range of ϕ-values (Fig. S13). In contrast, for all GROMOS96 trajectories we found a very broad sampling of ϕ/ψ pairs in the glycine Ramachandran plots, which are decomposed in several basins and deviate from empirical distributions obtained from a dihedral statistics as derived from the protein data bank (Fig. S11) (45). For proline residues the conformational preferences are restricted to the α_R and the PP_{II} regions due to steric constraints. Here, the obtained normalized Ramachandran plots are more similar among the compared force fields (Fig. S14). The occupancy of the PP_{II} region is high for all simulations conducted with the GROMOS96 and OPLS force fields. A more balanced relative sampling is found with ff03 and ff99SB, which is in agreement with the empirical PDB statistics for proline residues (Fig. S11) (45).
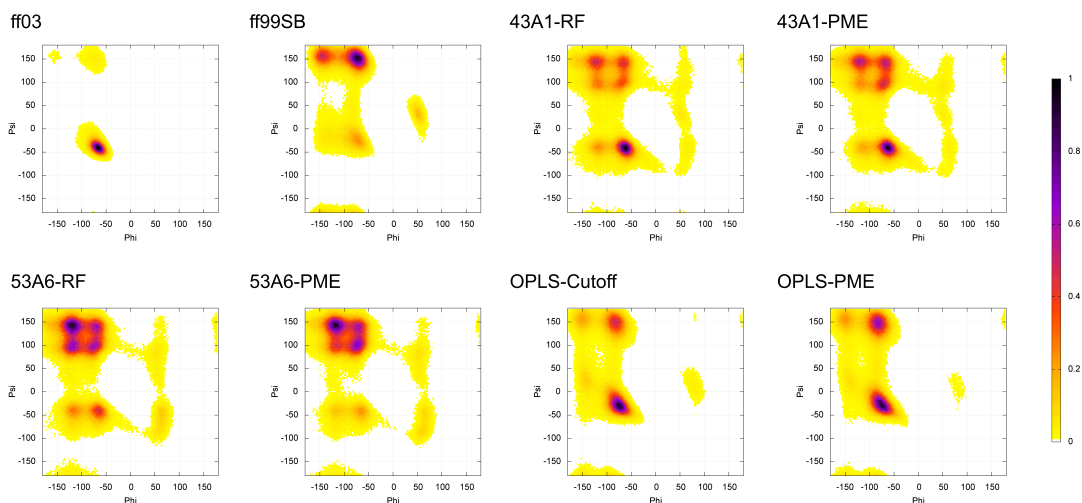
Figure 12: Normalized ϕ/ψ histogram plot for alanine residues obtained in the simulations with the various force fields.
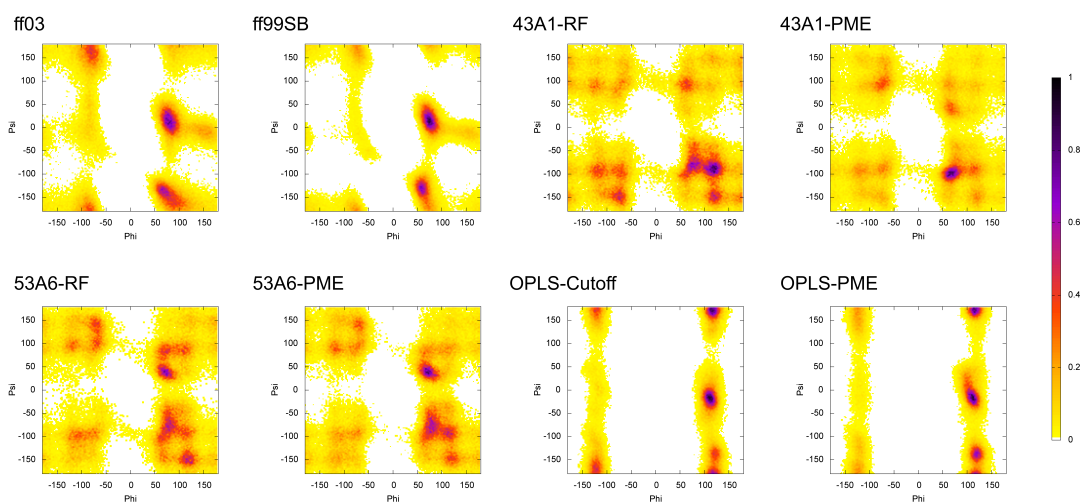

Figure 13: Normalized ϕ/ψ histogram plot for glycine residues obtained in the simulations with the various force fields.
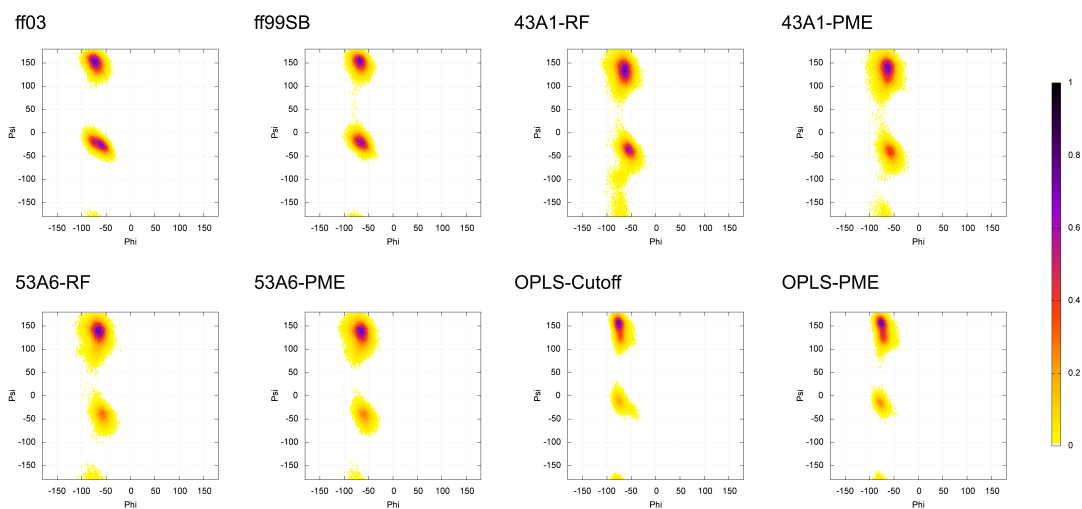

Figure 14: Normalized ϕ/ψ histogram plot for proline residues obtained in the simulations with the various force fields.

6   Principal Component Analysis (PCA)

In the PCA projections only one broadly and densely sampled area was found for all four ff99SB simulations, which is explained by only minor conformational changes (Fig. S15 *B*). In the projections of the trajectories obtained with both OPLS force field variants are mainly two visited states visible (see Fig. S15, *G* and *H*). A transition path to a more populated cluster of structures away from the reference was seen. The use of PME apparently decreased the frequency of larger conformational transitions, as only the 250 ns long TC5B.REF simulation with OPLS-PME visited this phase region (Fig. S15 *H*). In the Tc5b simulations with ff03, four states are sampled. One of them is exclusively visited in the 30 ns long TC5B.REF.3 simulation (Fig. S15 *A*, red point cloud), which also showed an increased RMSD over the last 15 ns. The simulations of the Trp-cage with the G96 force fields showed a overall similar trend in the PCA projections (Fig. S15, *C-F*). Although partially conformations close to the reference structure were visited, the simulations quickly explored different areas of the phase space, with most of them distinct from the NMR reference state. The projected conformational space is decomposed in many states and different for each of the four simulations. Moreover, the conformations with very little native contacts were already sampled within 30 ns in most of the cases, as indicated by the several short runs. In particular, conformational ensembles of the Trp-cage for both 53A6 variants evolved around the reference structure as a diffuse cloud of points (Fig. S15, *E* and *F*)
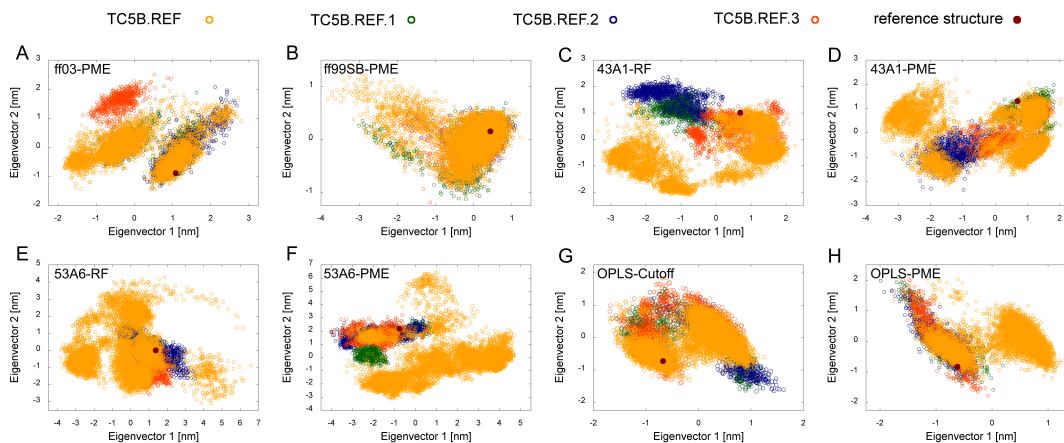

Figure 15: Conformational space sampled in the simulations of the Trp-cage (Tc5b). The reference structure is indicated by the dark-red dot. Snapshots from the 250 ns trajectory are shown with orange open circles (TC5B.REF). Conformtations of the three 30 ns simulations are depicted by green (TC5B.REF.1), dark-blue (TC5B.REF.2) and orange-red circles (TC5B.REF.3).

References

[1] Honda, S., K. Yamasaki, Y. Sawada, and H. Morii, 2004. 10 Residue Folded Peptide Designed by Segment Statistics. *Structure* 12:1507–1518.

[2] Seibert, M. M., A. Patriksson, B. Hess, and D. van der Spoel, 2005. Reproducible Polypeptide Folding and Structure Prediction using Molecular Dynamics Simulations. *J. Mol. Biol.* 354:173–183.

[3] Suenaga, A., T. Narumi, N. Futatsugi, R. Yanai, Y. Ohno, N. Okimoto, and M. Taiji, 2007. Folding Dynamics of 10-Residue beta-Hairpin Peptide Chignolin. *Chem. Asian J.* 2:591–598.

[4] van der Spoel, D., and M. M. Seibert, 2006. Protein Folding Kinetics and Thermodynamics from Atomistic Simulations. *Phys. Rev. Lett.* 96:238102.

[5] Satoh, D., K. Shimizu, S. Nakamura, and T. Terada, 2006. Folding free-energy landscape of a 10-residue mini-protein, chignolin. *FEBS Lett.* 580:3422–3426.

[6] Fedorov, D., T. Ishida, M. Uebayasi, and K. Kitaura, 2007. The Fragment Molecular Orbital Method for Geometry Optimizations of Polypeptides and Proteins. *J. Phys. Chem. A* 111:2722–2732.

[7] Xu, W., T. Lai, Y. Yang, and Y. Mu, 2008. Reversible folding simulation by hybrid Hamiltonian replica exchange. *J. Chem. Phys.* 128:175105–10.

[8] Pastor, M. T., M. L. de la Paz, E. Lacroix, L. Serrano, and E. Perez-Paya, 2002. Combinatorial approaches: A new tool to search for highly structured beta-hairpin peptides. *Proc. Nat. Acad. Sci.* 99:614–619.

[9] Neidigh, J. W., R. M. Fesinmeyer, and N. H. Andersen, 2002. Designing a 20-residue protein. *Nat. Struct. Mol. Biol.* 9:425–430.

[10] Qiu, L., S. A. Pabit, A. E. Roitberg, and S. J. Hagen, 2002. Smaller and Faster: The 20-Residue Trp-Cage Protein Folds in 4 mus. *J. Am. Chem. Soc.* 124:12952–12953.

[11] Zhou, R., 2003. Trp-cage: Folding free energy landscape in explicit water. *Proc. Nat. Acad. Sci.* 100:13280–13285.

[12] Nikiforovich, G. V., N. H. Andersen, R. M. Fesinmeyer, and C. Frieden, 2003. Possible locally driven folding pathways of TC5b, a 20-residue protein. *Protein Struct. Funct. Gene* 52:292–302.

[13] Ulmschneider, J. P., M. B. Ulmschneider, and A. Di Nola, 2006. Monte Carlo vs Molecular Dynamics for All-Atom Polypeptide Folding Simulations. *J. Phys. Chem. B* 110:16733–16742.

[14] Simmerling, C., B. Strockbine, and A. E. Roitberg, 2002. All-Atom Structure Prediction and Folding Simulations of a Stable Protein. *J. Am. Chem. Soc.* 124:11258–11259.

[15] Snow, C. D., B. Zagrovic, and V. S. Pande, 2002. The Trp Cage Folding Kinetics and Unfolded State Topology via Molecular Dynamics Simulations.

[16] Lockhart, D. J., and P. S. Kim, 1992. Internal Stark Effect Measurement of the Electric Field at the Amino Terminus of an alpha-Helix. *Science* 257:947–951.

[17] Lockhart, D. J., and P. S. Kim, 1993. Electrostatic Screening of Charge and Dipole Interactions with the Helix Backbone. *Science* 260:198–202.

[18] Williams, S., T. Causgrove, R. Gilmanshin, K. Fang, R. Callender, W. Woodruff, and R. Dyer, 1996. Fast Events in Protein Folding: Helix Melting and Formation in a Small Peptide. *Biochemistry* 35:691–697.

[19] Thompson, P., W. Eaton, and J. Hofrichter, 1997. Laser Temperature Jump Study of the Helix Coil Kinetics of an Alanine Peptide Interpreted with a 'Kinetic Zipper' Model. *Biochemistry* 36:9200–9210.

[20] Lednev, I., A. Karnoup, M. Sparrow, and S. Asher, 1999. alpha-Helix Peptide Folding and Unfolding Activation Barriers: A Nanosecond UV Resonance Raman Study. *J. Am. Chem. Soc.* 121:8074–8086.

[21] Asher, S., A. Mikhonin, and S. Bykov, 2004. UV Raman Demonstrates that alpha-Helical Polyalanine Peptides Melt to Polyproline II Conformations. *J. Am. Chem. Soc.* 126:8433–8440.

[22] Garcia, A. E., and K. Y. Sanbonmatsu, 2002. alpha-Helical stabilization by side chain shielding of backbone hydrogen bonds. *Proc. Nat. Acad. Sci.* 99:2782–2787.

[23] Nymeyer, H., and A. E. Garcia, 2003. Simulation of the folding equilibrium of alpha-helical peptides: A comparison of the generalized Born approximation with explicit solvent. *Proc. Nat. Acad. Sci.* 100:13934–13939.

[24] Gnanakaran, S., and A. Garcia, 2003. Validation of an All-Atom Protein Force Field: From Dipeptides to Larger Peptides. *J. Phys. Chem. B* 107:12555–12557.

[25] Zhang, W., H. Lei, S. Chowdhury, and Y. Duan, 2004. Fs-21 Peptides Can Form Both Single Helix and Helix-Turn-Helix. *J. Phys. Chem. B* 108:7479–7489.

[26] Gnanakaran, S., and A. E. Garcia, 2005. Helix-coil transition of alanine peptides in water: Force field dependence on the folded and unfolded structures. *Protein Struct. Funct. Bioinf* 59:773–782.

[27] Sorin, E. J., and V. S. Pande, 2005. Exploring the Helix-Coil Transition via All-Atom Equilibrium Ensemble Simulations. *Biophys. J.* 88:2472–2493.

[28] Sorin, E. J., and V. S. Pande, 2005. Empirical force-field assessment: The interplay between backbone torsions and noncovalent term scaling. *J. Comput. Chem.* 26:682–690.

[29] Gnanakaran, S., H. Nymeyer, J. Portman, K. Y. Sanbonmatsu, and A. E. Garcia, 2003. Peptide folding simulations. *Cur. Opin. Struct. Biol.* 13:168–174.

[30] Munoz, V., and L. Serrano, 1994. Elucidating the folding problem of helical peptides using empirical parameters. *Nat. Struct. Mol. Biol.* 1:399–409.

[31] Hornak, V., R. Abel, A. Okur, B. Strockbine, A. Roitberg, and C. Simmerling, 2006. Comparison of multiple Amber force fields and development of improved protein backbone parameters. *Protein Struct. Funct. Bioinf* 65:712–725.

[32] Wang, R., J.and Cieplak, and P. Kollman, 2000. *J. Comp. Chem.* 21:1049–1074.

[33] Duan, Y. et al., 2003. A point-charge force field for molecular mechanics simulations of proteins based on condensed-phase quantum mechanical calculations. *J. Comput. Chem.* 24:1999–2012.

[34] Jorgensen, W., D. Maxwell, and J. Tirado-Rives, 1996. Development and Testing of the OPLS All-Atom Force Field on Conformational Energetics and Properties of Organic Liquids. *J. Am. Chem. Soc.* 118:11225–11236.

[35] Kaminski, G., R. Friesner, J. Tirado-Rives, and W. Jorgensen, 2001. Evaluation and Reparametrization of the OPLS-AA Force Field for Proteins via Comparison with Accurate Quantum Chemical Calculations on Peptides. *J. Phys. Chem. B* 105:6474–6487.

[36] van Gunsteren, W. F., S. R. Billeter, A. A. Eising, P. H. Hünenberger, P. Krüger, A. E. Mark, W. R. P. Scott, and I. G. Tironi, 1996. Biomolecular Simulation: The GROMOS96 manual and user guide. Hochschulverlag AG an der ETH Zürich, Zürich, Switzerland.

[37] Scott, W., P. Hunenberger, I. Tironi, A. Mark, S. Billeter, J. Fennen, A. Torda, T. Huber, P. Kruger, and W. van Gunsteren, 1999. The GROMOS Biomolecular Simulation Program Package. *J. Phys. Chem. A* 103:3596–3607.

[38] Oostenbrink, C., A. Villa, A. E. Mark, and W. F. V. Gunsteren, 2004. A biomolecular force field based on the free enthalpy of hydration and solvation: The GROMOS force-field parameter sets 53A5 and 53A6. *J. Comput. Chem.* 25:1656–1676.

[39] Oostenbrink, C., T. A. Soares, N. F. A. van der Vegt, and W. F. van Gunsteren, 2005. Validation of the 53A6 GROMOS force field. *Eur. Biophys. J.* 34:273–284.

[40] Darden, T., D. York, and L. Pedersen, 1993. Particle mesh Ewald: An N-log(N) method for Ewald sums in large systems. *J. Chem. Phys.* 98:10089–10092.

[41] Essmann, U., L. Perera, M. L. Berkowitz, T. Darden, H. Lee, and L. G. Pedersen, 1995. A smooth particle mesh Ewald method. *J. Chem. Phys.* 103:8577–8593.

[42] Tironi, I. G., R. Sperb, P. E. Smith, and W. F. van Gunsteren, 1995. A generalized reaction field method for molecular dynamics simulations. *J. Chem. Phys.* 102:5451–5459.

[43] G. N. Ramachandran, C. Ramakrishnan und V. Sasisekharan, *J. Mol. Biol.*, **1963**, *7*, 95–99.

[44] C. Ramakrishnan und G. N. Ramachandran, *Biophys. J.*, **1965**, *5*, 909–933.

[45] S. C. Lovell, I. W. Davis, W. B. Arendalll III, P. I. W. de Bakker, J. M. Word, et al., *Proteins*, **2003**, *50*, 437–450.